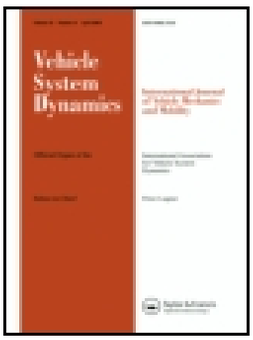

Vehicle System Dynamics

ISSN: 0042-3114 (Print) 1744-5159 (Online) Journal homepage: https://www.tandfonline.com/loi/nvsd20

Magic Formula Tyre Model with Transient Properties

H. B. PACEJKA & I. J. M. BESSELINK

To cite this article: H. B. PACEJKA & I. J. M. BESSELINK (1997) Magic Formula Tyre Model with Transient Properties, Vehicle System Dynamics, 27:S1, 234-249, DOI: 10.1080/00423119708969658

To link to this article: https://doi.org/10.1080/00423119708969658

Vehicle System Dynamics Supplement 27 (1997), pp. 234-249

Magic Formula Tyre Model with Transient Properties

H. B. PACEJKA and I. J. M. BESSELINK

ABSTRACT

The tyre force and moment generating properties connected with the vehicle's horizontal motions are considered. Knowledge of tyre properties is necessary to properly design vehicle components and advanced control systems. For this purpose, mathematical models of the tyre are being used in vehicle simulation models. The steady-state empirical 'Magic Formula tyre model' is discussed. The aligning torque description is based on the concepts of pneumatic trail and residual torque. This facilitates its combined slip description. Following Michelin, weighting functions have been introduced to model the combined slip force generation. A full set of equations of the steady-state part of the model of the new version 'Delft Tyre 97' is presented. The non-steady state behaviour of the tyre is of importance in rapid transient maneuvres, when cornering on uneven roads and for the analysis of oscillatory braking and steering properties. A relatively simple model for longitudinal and lateral transient responses restricted to relatively low time and path frequencies is introduced.

INTRODUCTION

The widely used empirical tyre model, the newest version of which is presented here, is based on the so-called Magic Formula. The development of the model was started in the mid-eighties. In a cooperative effort TU-Delft and Volvo developed several versions (1987, 1989, 1991). In these models the combined slip situation was modelled from a physical view point. In 1993 Michelin introduced a purely empirical method using Magic Formula based functions to describe the tyre horizontal force generation at combined slip. In the previous version of 'Delft Tyre' this approach was adopted and the original description of the aligning torque has been altered to accommodate a relatively simple combined slip extension (cf. [11]). The model presented here is not restricted to small values of slip and the wheel may run backwards. A complete description of the steady-state response is given in the Appendix. The description of transient and oscillatory properties of the tyre-wheel combination has been improved. The dynamic behaviour may be covered by the model as long as the frequency of the wheel motion remains well below the first natural frequencies of the belt with respect to the rim (i.e. < ca. 15Hz) and if the wavelength of motion and road undulation is sufficiently large with respect to the tyre contact length (i.e. > ca. 1.5m).

STEADY-STATE MODEL FOR PURE SLIP

We refer to [3] for a detailed treatment of the pure slip part of this model (that is: at either lateral slip α or longitudinal slip κ). For the side force F_y and the fore and aft force F_x that part of the model remained unchanged. The formula reads:

$$y = D \sin[C \arctan\{Bx - E(Bx - \arctan Bx)\}] \tag{1}$$

with

$$\begin{aligned} Y(X) &= y(x) + S_v \\ x &= X + S_h \end{aligned} \tag{2}$$

where

- Y: output variable F_x or F_y
- X: input variable α or κ

and

- B: stiffness factor
- C: shape factor
- D: peak value
- E: curvature factor
- S_H: horizontal shift
- S_V: vertical shift

The Magic Formula $y(x)$ typically produces a curve that passes through the origin $x=y=0$, reaches a maximum and subsequently tends to a horizontal asymptote. For given values of the coefficients B, C, D and E the curve shows an anti-symmetric shape with respect to the origin. To allow the curve to have an off-set with respect to the origin two shifts S_H and S_V have been introduced. A new set of coordinates $Y(X)$ arises as shown in Fig. 1.

The formula is capable of producing characteristics that closely match measured curves for the side force F_y and the fore and aft force F_x as functions of their respective wheel slip quantities:lateral slip α and longitudinal slip κ. Note that in this presentation α represents the tangent of the slip angle; at small lateral slip the difference is negligible.

Figure 1 (upper part) illustrates the meaning of some of the factors with the help of a typical side force characteristic. Obviously, coefficient D represents the peak value (with respect to the x-axis) and the product BCD corresponds to the slope at the origin ($x=y=0$). The shape factor C controls the limits of the range of the sine function appearing in the formula (1) and thereby determines the shape of the resulting curve. The factor B is left to determine the slope

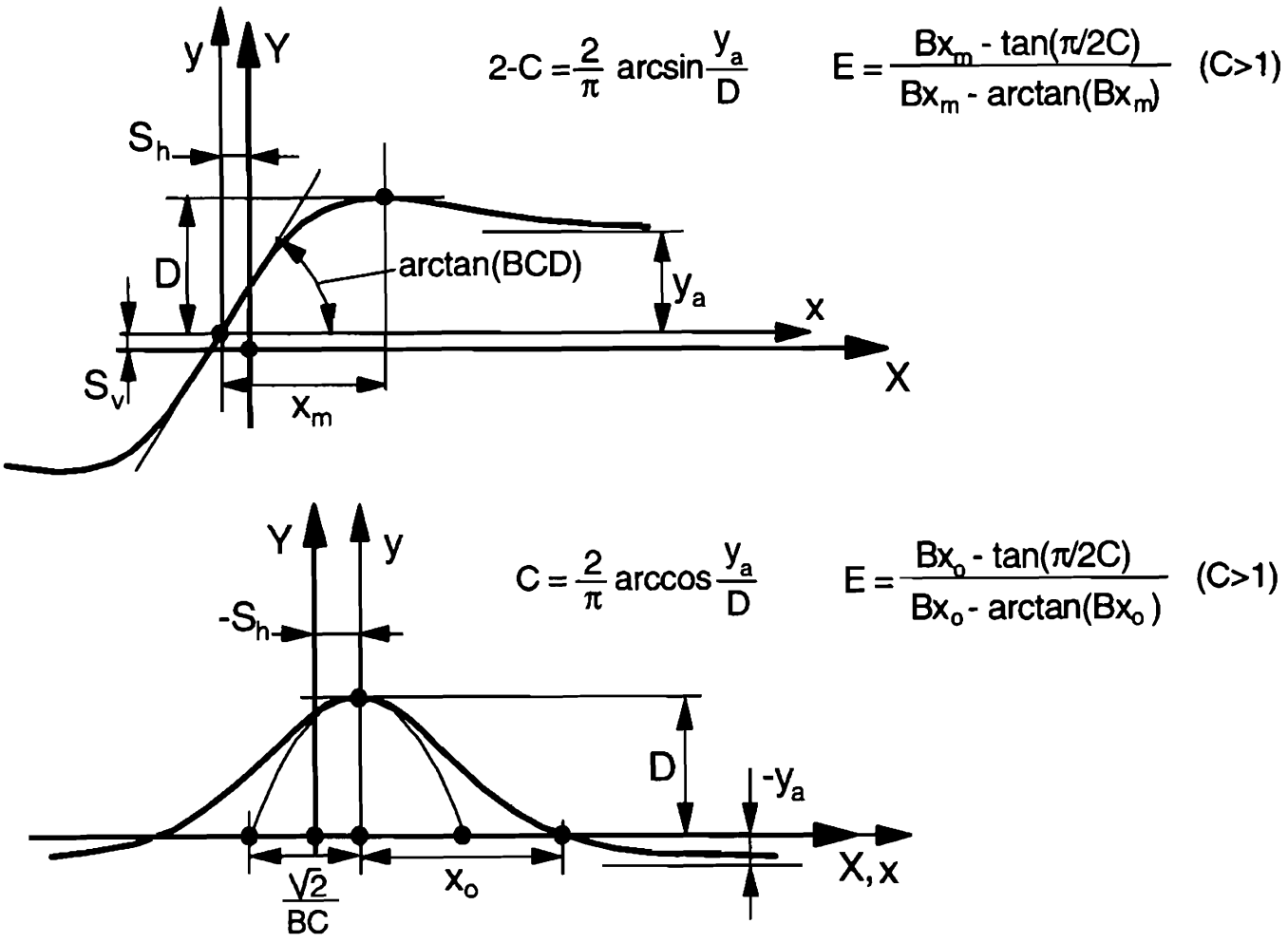

Fig. 1. Curves produced by the sine and cosine versions of the Magic Formula, Eqs.(1) and (6). Meaning of curve parameters have been indicated.

at the origin and is called the stiffness factor. The offsets S_H and S_V appear to occur when ply-steer and conicity effects and possibly the rolling resistance cause the F_y and F_x curves not to pass through the origin. Also, wheel camber will give rise to a considerable offset of the F_y vs α curves. Such a shift may be accompanied by a significant deviation from the pure anti-symmetric shape of the original curve. To accommodate such an asymmetry, the curvature factor E is made dependent of the sign of the abscissa (x).

$$E = E_o + \Delta E \cdot \mathrm{sgn}(x) \tag{3}$$

Also the difference in shape that is expected to occur in the F_x vs κ characteristic between the driving and braking ranges can be taken care of.

The various factors are given functions of normal load and wheel camber angle. A number of parameters appears in these functions. A suitable regression technique is used to determine their values from measured data corresponding to the best fit (cf. [4]). One of the important

functional relationships used is the load dependency of the cornering stiffness (or approximately: $BCD_y=\partial F_y/\partial\alpha$ at $\alpha+S_{Hy}=0$).

$$BCD_y = K_y = p_{Ky1}\sin[2\arctan(F_z/p_{Ky2})]\cdot(1-p_{Ky3}|\gamma|) \tag{4}$$

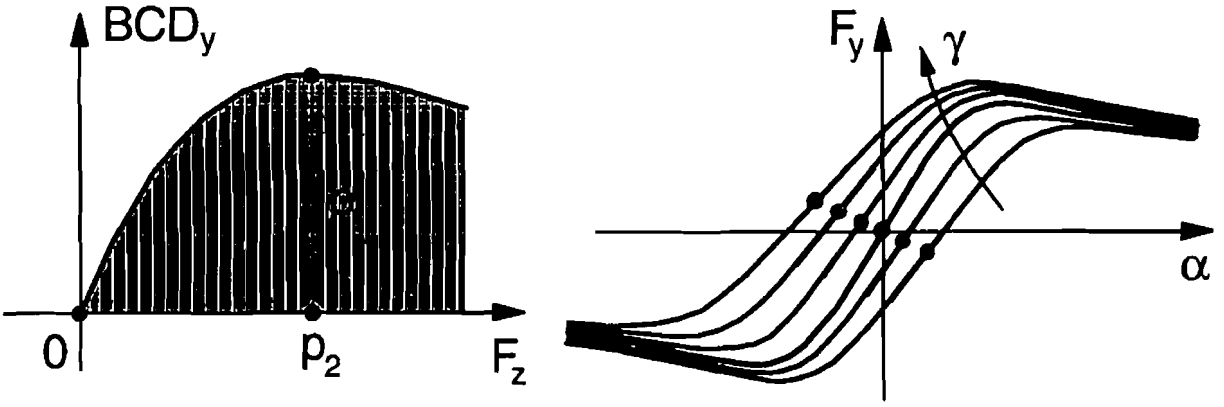

Fig. 2. Cornering stiffness versus vertical load and the influence of wheel camber, Eq. (4).

For zero camber, the cornering stiffness attains its maximum p_{Ky1} at $F_z=p_{Ky2}$. In Fig. 2 the basic relationship has been depicted. Apparently, for a cambered wheel the cornering stiffness is decreased.

The aligning torque M_z can now be obtained by multiplying the side force F_y with the pneumatic trail t and adding the usually small residual torque M_{zr} (Fig. 3). We have:

$$M_z = -t\cdot F_y + M_{zr} \tag{5}$$

with the pneumatic trail

$$t(\alpha_t) = D_t\cos[C_t\arctan\{B_t\alpha_t - E_t(B_t\alpha_t - \arctan(B_t\alpha_t))\}]\cdot c_\alpha \tag{6}$$

$$\alpha_t = \alpha + S_{Ht} \tag{7}$$

$$M_{zr}(\alpha_r) = D_r\cos[\arctan(B_r\alpha_r)]\cdot c_\alpha \tag{8}$$

$$\alpha_r = \alpha + S_{Hf} \tag{9}$$

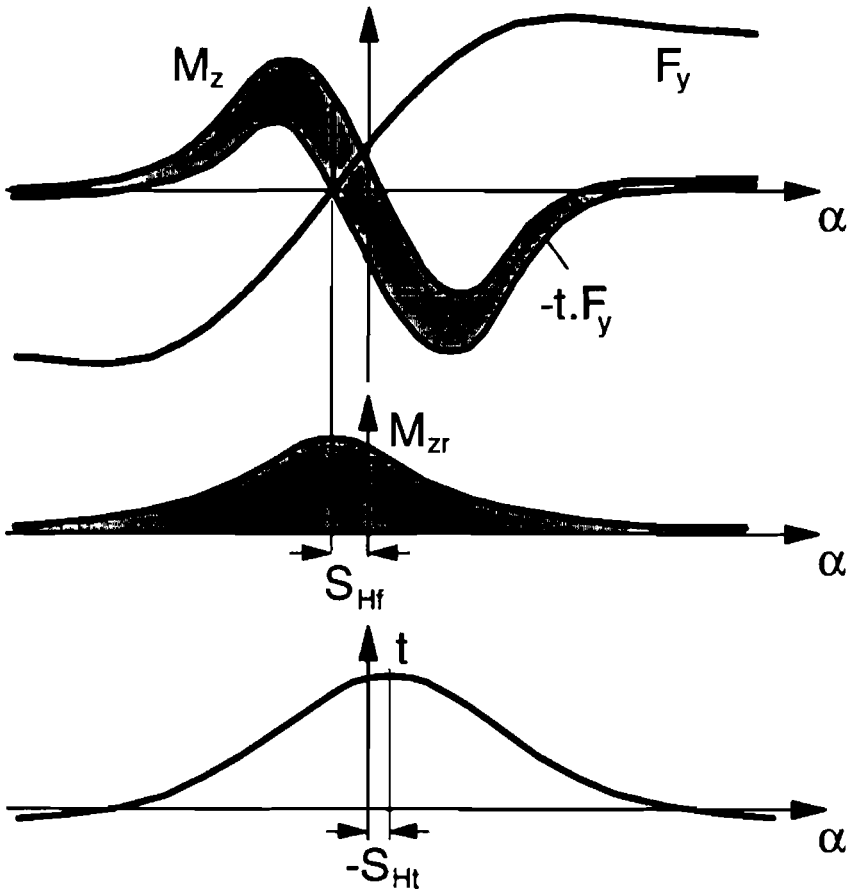

Fig. 3. Aligning torque characteristic produced by adding two parts: the product of side force and pneumatic trail and the residual torque, Eq. (7) .

It is seen that both parts of the moment have been modelled using the Magic Formula, but instead of the sine function, the cosine function has been employed. In that way a hill-shaped curve is produced. In the Appendix more complete formulae are given including the consequence of running backwards.

In Fig. 1 (lower part) the basic properties of the cosine M.F. curve have been indicated (subscripts of factors deleted). Again, D is the peak value, C is a shape factor determining the level of the horizontal asymptote and now B influences the curvature at the peak (illustrated with the parabola). Factor E changes the shape at larger values of slip. The residual torque attains its maximum D_r at the slip angle where the side force becomes equal to zero. This is accomplished through the horizontal shift S_{Hf}. The peak of the pneumatic trail occurs at $\alpha = -S_{Ht}$. This formulation has proven to give excellent agreement with measured curves. The advantage with respect to the earlier versions where formula (3) is used for the aligning torque as well, is that we have now directly assessed the pneumatic trail which is needed (as in the previous version [3]) for handling the combined slip situation.

STEADY-STATE MODEL FOR COMBINED SLIP

In [3] the tyre's response to combined slip was modelled by using physically based formulae. A newer more efficient way is purely empiric. This method was developed by Michelin and published in [5]. It describes the effect of combined slip on both the lateral and the longitudinal forces. Weighting functions G are introduced which when multiplied with the original pure slip functions (that is Eq.(3)) produce the interactive effects of κ on F_y and of α on F_x. The weighting functions have a hill shape. They should take the value one in the special case of pure slip (κ or α equal to zero). When, for example, at a given slip angle a from zero increasing brake slip is introduced, the relevant weighting function for F_y may first show a slight increase in magnitude (becoming larger than one) but will soon reach its peak after which a continuous decrease follows. The cosine version of the Magic Formula is used to represent the hill shaped function:

$$G = D\cos[C\arctan(Bx)] \tag{10}$$

Here, G is the resulting weighting factor and x is either κ or α (possibly shifted). The coefficient D represents the peak value (slightly deviating from one if a horizontal shift of the hill occurs), C determines the level of the hill's base and B influences the sharpness of the hill. Apparently, the factor E was not needed to improve the fit. For the side force we obtain the following formulae:

$$F_y = G_{y\kappa}\cdot F_{yo} + S_{Vy\kappa} \tag{11}$$

$$G_{y\kappa} = \frac{\cos[C_{y\kappa}\arctan\{B_{y\kappa}(\kappa + S_{Hy\kappa})\}]}{\cos[C_{y\kappa}\arctan(B_{y\kappa}S_{Hy\kappa})]} \tag{12}$$

$$B_{y\kappa} = r_{By1}\cos[\arctan\{r_{By2}(\alpha - r_{By3})\}] \tag{13}$$

$$S_{Vy\kappa} = D_{Vy\kappa}\sin[r_{Vy5}\arctan(r_{Vy6}\kappa)] \tag{14}$$

In Eq.(11) F_{yo} denotes the side force at pure side slip obtained from Eq.(1); $S_{Vy\kappa}$ is the vertical shift sometimes referred to as the κ-induced ply-steer. This function varies with longitudinal slip κ as indicated in Eq.(14). Its maximum $D_{Vy\kappa}$ decreases with increasing magnitude of the slip angle (cf. App.). The factor $B_{y\kappa}$ influences the sharpness of the hill shaped weighting function (12). As indicated, the hill becomes more shallow (wider) at larger slip angles (then $B_{y\kappa}$ decreases according to Eq.(13)). The other coefficients r appearing in the formulae are treated as constant parameters. The combined slip relations for F_x are similar. However, a vertical shift was not needed to be included. In Fig. 4 a three-dimensional graph is shown

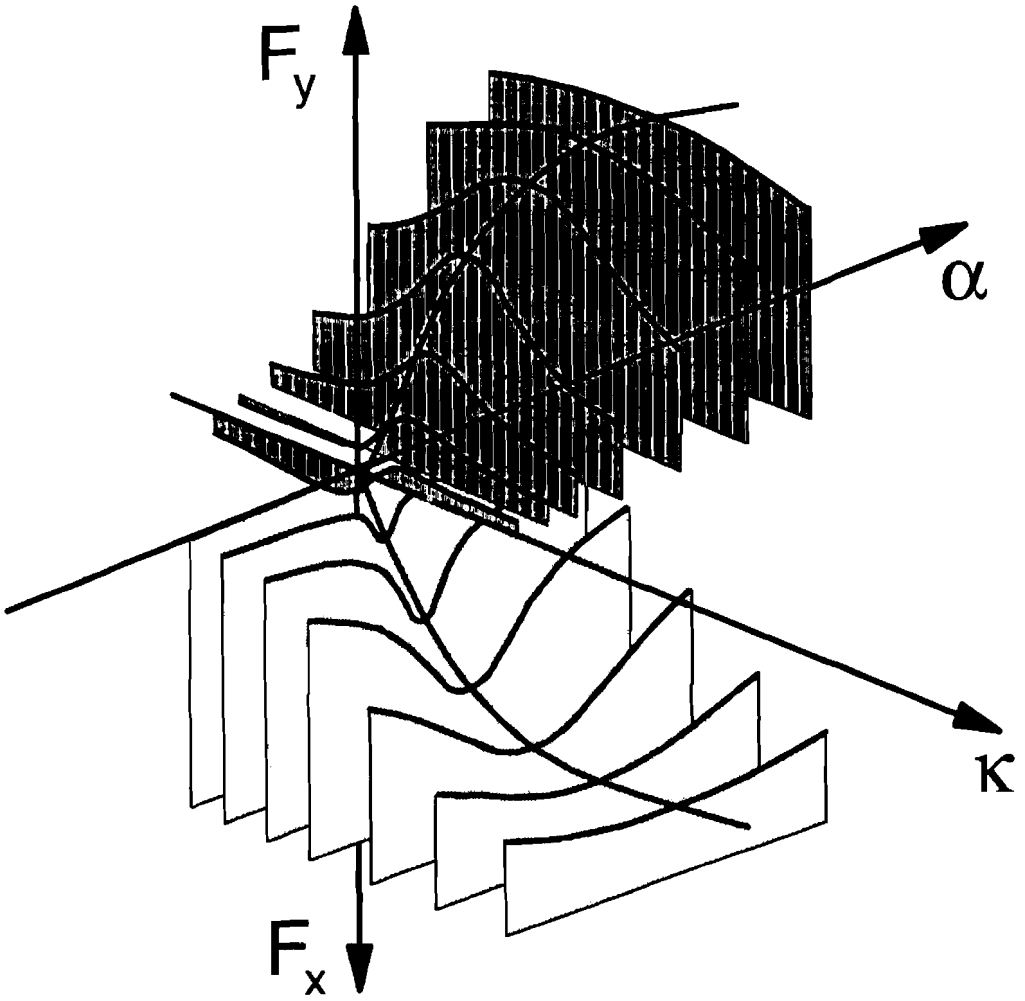

Fig. 4. Combined slip lateral and longitudinal force 3-D diagram showing the interaction of both slip components.

indicating the variation of F_x and F_y with both α and κ.

Regarding the aligning torque, physical insight has been employed to model the situation at combined slip. The arguments α_t and α_f (including a shift) appearing in the functions for pneumatic trail and residual torque are replaced by equivalent lateral slip quantities incorporating the effect of κ on the composite slip level. Besides, an extra term is included to account for the fact that an additional moment arm s arises for F_x as a result of camber γ and lateral tyre deflections through F_y (similar to the model description of [3]). The latter fact may give rise to a sign change of the aligning torque in the range of braking.

$$M_z = -t(\alpha_{t,eq}) \cdot F_y + M_{zr}(\alpha_{r,eq}) + s(F_y, \gamma) \cdot F_x \qquad \textbf{(15)}$$

$$\alpha_{t,eq} = \sqrt{\alpha_t^2 + \left(\frac{K_x}{K_y}\right)^2 \kappa^2} \cdot \mathrm{sgn}(\alpha_t) \tag{16}$$

and similar for $\alpha_{r,eq}$.

As mentioned before, the complete set of steady-state formulae has been listed in the Appendix. Parameters p, q, r and s of the model are non-dimensional quantities. In addition, user scaling factors λ have been introduced. With that tool the effect of changing friction coefficient, cornering stiffness, camber stiffness etc. can be quickly investigated in a qualitative way without having the need to implement a completely new tyre data set. Scaling is done in such a way that realistic relationships are maintained. For instance, when changing the cornering stiffness and the friction coefficient in lateral direction (through λ_{Ky} and $\lambda_{\mu y}$), the abscissa of the pneumatic trail characteristic is changed in a way similar to that of the side force characteristic.

MODEL FOR TRANSIENT RESPONSE

In previous publications, the concept of the relaxation length was employed to account for the compliance of the carcass with respect to the rim that is responsible for the lag in the response to lateral and longitudinal slip (cf. Refs. [6,7]). For small values of slip this way of approach is adequate. At larger slip levels, the lag deminishes according to experimental evidence. Also to avoid carcass deflections becoming too large, relaxation lengths may be introduced that decrease with increasing contact line deformation gradients [7]. The computations, however, become cumbersome due to possible instabilities and the situation at combined slip may become complex.

Therefore, another way to attack the problem is introduced. A contact patch is defined that can deflect horizontally with respect to the lower part of the rim. Only translations are allowed relative to the wheel plane. A mass point is attached to the moving contact patch to enable the calculation of the forces F_x^* and F_y^* and the moment M_z^* acting between road and tyre as a response to the slip velocity V_s^* of the mass point and to the camber angle. The effect of turn slip has not been taken into account.

It is assumed that this response to contact patch slip motions is instantaneous because a deflection is not needed to be developed here. In [8] this approach was adopted to model the longitudinal and circumferential dynamics of the tyre wheel combination in an attempt to study the effect of road undulations on anti-lock brake control. It may be noted that the carcass compliance together with the slip model of the contact patch automatically takes care of the wheel load dependent lag and also of the decrease in lag at increased (combined) slip. Figure 5 shows the model configuration in top and side view.

In addition, the contribution of three important gyroscopic effects related with belt distorsions are taken into account: the gyroscopic couple M_{zgyr} due to the rate of change of the lateral tyre deflection $\dot{v}_c$, the slip angle induced by this couple (through belt yaw distorsion) and the effect of the wheel yaw rate induced gyroscopic couple about the x-axis that acts on the tyre deflection v_c through the internal force F_{ygyr}. Moreover, the non-lagging part of the camber force is modelled to act directly on the wheel rim. Consequently, this part $F_{y\gamma NL}$ is first subtracted from the ground force F_y^*. The non-lagging part (i.e. the instantaneous response to pure camber variations) is a fraction of the total camber force. Sometimes negative fractions have been observed to occur [10].

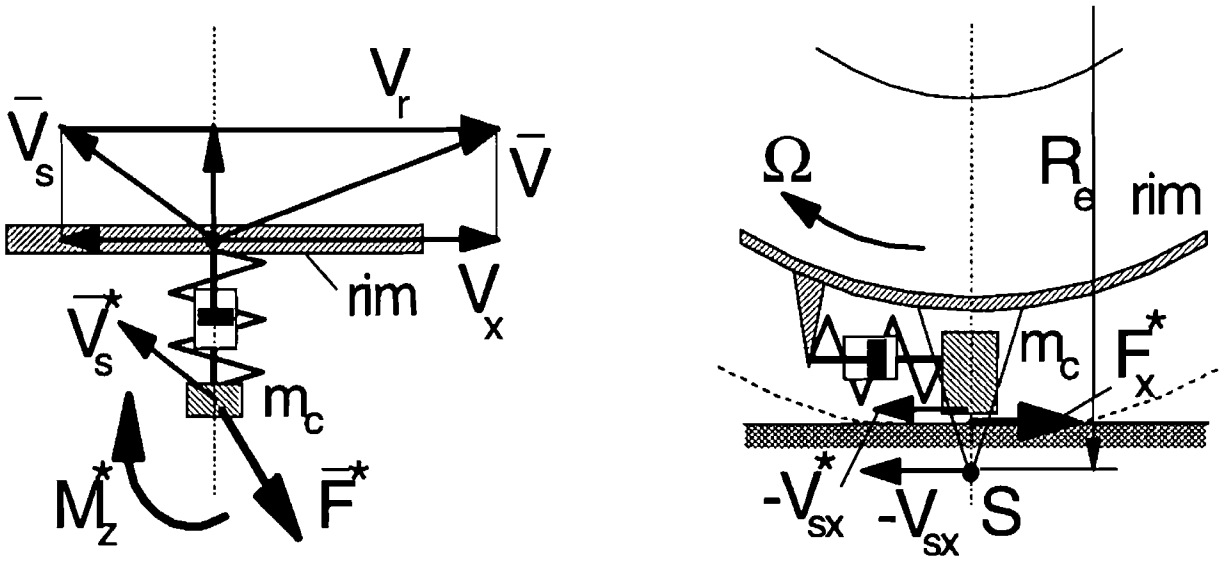

Fig. 5. Tyre model in top and side view, showing deflected contact patch with mass m_c.

The equations for the relative longitudinal and lateral motions u_c and v_c of the contact patch mass m_c with simplified acceleration terms read:

$$m_c\ddot{u}_c + k_{Fx}\dot{u}_c + c_{Fx}u_c = F_x^* \tag{17}$$

$$m_c\ddot{v}_c + k_{Fy}\dot{v}_c + c_{Fy}v_c = F_y^* - F_{y\gamma NL} + F_{ygyr} \tag{18}$$

Stiffnesses of the lower part of the carcass as measured on the standing tyre are introduced as well as damping coefficients. Damping may be needed to avoid self-excited vibrations when operating in ranges of slip where the characteristic slopes down with increasing slip. The slip velocity vector of the contact patch reads:

$$\bar{V}_s^* = \bar{V}_s + \begin{pmatrix} \dot{u}_c \\ \dot{v}_c - V_x\psi_{gyr} \end{pmatrix} \tag{19}$$

and the slip vector of the contact patch:

$$\begin{pmatrix} \kappa^* \\ \alpha^* \end{pmatrix} = -\frac{\bar{V}_s^*}{|V_x|} \tag{20}$$

where $|V_x|$ denotes the absolute value of the forward component of the velocity of the wheel centre (or better: of the contact centre or point of intersection). The slip speed V_s of the wheel rim is defined as the horizontal velocity of slip point S that is attached to the rim a distance R_e (the effective rolling radius) below the wheel centre (Fig. 5).
The horizontal forces $F_{x,y}^*$ and the moment M_z^* may now be calculated as steady-state responses (cf. Appendix) to the slip of the contact patch. After that, the forces $F_{x,y}$ and the moment M_z of interest (which are supposed to act on the assumedly rigid tyre wheel disc) are calculated as follows:

$$F_x = F_x^* - m_c \ddot{u}_c \tag{21}$$

$$F_y = F_y^* - m_c \ddot{v}_c \tag{22}$$

$$M_z = M_z^* + M_{zgyr} \tag{23}$$

The following expressions hold for the various quantities introduced.

$$F_{y\gamma NL} = F_z(p_{Ty8} + p_{Ty9} df_z) \cdot \gamma \tag{24}$$

with df_z the normalized load increase (cf. App. Eq.(30)).

$$M_{zgyr} = -c_{zgyr} R_o m_t \Omega \dot{v}_c \tag{25}$$

with R_0 the wheel radius, m_t the tyre mass, Ω the wheel speed of revolution.

$$F_{ygyr} = c_{ygyr} R_o m_t \Omega \frac{d\psi}{dt} \tag{26}$$

with ψ the wheel yaw angle.

$$\psi_{gyr} = c_{\psi gyr} \frac{M_{zgyr}}{R_o^2 c_{Fy}} \tag{27}$$

For a steel belted radial car tyre the non-dimensional coefficients c_{zgyr}, c_{ygyr} and $c_{\psi gyr}$ may all be estimated to be approximately equal to 0.5. The lateral stiffness c_{Fy} may be obtained by using its relation with the relaxation length σ_α through the cornering stiffness $C_{F\alpha}$ (=K_y).

$$\sigma_\alpha = \frac{C_{F\alpha}}{c_{Fy}} \tag{28}$$

Various types of motions have been simulated using the model. Limited space does not allow us to present results and discuss the performance of the model.

REFERENCES

1. H.B. Pacejka and R.S. Sharp, 'Shear force development by pneumatic tyres in steady state conditions: A review of modelling aspects'. Veh.Sys.Dyn. 20 (1991), pp. 121-176.
2. W.R. Pasterkamp and H.B. Pacejka, 'On-line estimation of tyre characteristics for vehicle control'. AVEC '94, Japan, Oct. 1994.
3. H.B. Pacejka and E. Bakker, 'The Magic Formula tyre model'. Proceedings 1st Tyre Colloquium, Delft, Oct.1991, Suppl. to Veh.Sys.Dyn., Vol. 21, 1993.
4. J. van Oosten and E. Bakker, 'Determination of Magic Formula tyre model parameters'. Proceedings 1st Tyre Colloquium, Delft, Oct. 1991, Suppl. to Veh.Sys.Dyn., Vol. 21, 1993.
5. P. Bayle, J.F. Forissier and S. Lafon, 'A new tyre model for vehicle dynamics simulations'. Automotive Technology International '93, pp. 193-198.
6. H.B. Pacejka, 'In-plane and out-of-plane dynamics of pneumatic tyres'. Veh.Sys.Dyn. 10 (1981), pp. 221-251.
7. H.B. Pacejka and T. Takahashi, 'Pure slip characteristics of tyres on flat and on undulated road surfaces'. AVEC '92, Yokohama, Sept. 1992.
8. P. van der Jagt, H.B. Pacejka and A.R. Savkoor, 'Influence of tyre and suspension dynamics on the braking performance of an anti-lock system on uneven roads'. EAEC Conf. '89, C382/047, IMechE 1989.
9. P.W.A. Zegelaar and H.B. Pacejka, 'In-plane dynamics of tyres on uneven roads', Proc. 14th IAVSD Symposium, Ann Arbor, Aug. 1995, Suppl. to Veh.Sys.Dyn., 1996.
10. A. Higuchi and H.B. Pacejka, 'The relaxation length concept at large wheel slip and camber'. This Proceedings.
11. H.B. Pacejka, 'The Tyre as a Vehicle Component'. Proc. XXVI FISITA Congress, 1996 (CD-Rom).

APPENDIX Delft Tyre 97 (steady-state part)

Superscript * refers to velocities and forces connected with the contact patch mass. Disregard this if only steady-state responses are required. Non-dimensional model parameters p, q, r and s have been introduced. For the user's convenience a set of scaling factors λ is available to examine the influence of changing a number of important overall parameters. The default value of these factors is set equal to one. We define in addition:

V magnitude of speed of wheel (contact centre) (≥ 0),
V_x forward component of speed of wheel (contact centre),
V_r ($=R_e\Omega=V_x-V_{sx}$) forward speed of rolling,
R_o unloaded tyre radius,
R_e effective rolling radius,
Ω wheel speed of revolution
ρ tyre radial deflection,
F_{zo} nominal load (≥ 0),
F'_{zo} adapted nominal load

$$F'_{zo} = \lambda_{F_{zo}} F_{zo} \tag{29}$$

df_z the normalized vertical load increment

$$df_z = \frac{F_z - F'_{zo}}{F'_{zo}} \tag{30}$$

$|V'_x|$ downward limited absolute forward wheel speed

$$|V'_x| = \max(|V_x|, \epsilon_x), \qquad (\epsilon_x = 0.01) \tag{31}$$

κ^* longitudinal slip of contact patch (protected against singularity)

$$\kappa^* = -\frac{V^*_{sx}}{|V'_x|} \tag{32}$$

α^* lateral slip of contact patch (protected against singularity)

$$\alpha^* = -\frac{V^*_{sy}}{|V'_x|} \tag{33}$$

V' downward limited speed V

$$V' = \max(V, \epsilon_x), \qquad (\epsilon_x = 0.01) \tag{34}$$

c_α =cosine of slip angle (protected against singularity)

$$c_\alpha = \frac{V_x}{V'} \tag{35}$$

Longitudinal Force (pure longitudinal slip)

$$F_{xo}^* = D_x \sin[C_x \arctan\{B_x\kappa_x - E_x(B_x\kappa_x - \arctan(B_x\kappa_x))\}] + S_{Vx} \tag{36}$$

$$\kappa_x = \kappa^* + S_{Hx} \tag{37}$$

$$C_x = p_{Cx1} \cdot \lambda_{Cx} \qquad (>0) \tag{38}$$

$$D_x = \mu_x \cdot F_z \tag{39}$$

$$\mu_x = (p_{Dx1} + p_{Dx2} df_z) \cdot \lambda_{\mu x} \qquad (>0) \tag{40}$$

$$E_x = (p_{Ex1} + p_{Ex2} df_z + p_{Ex3} df_z^2) \cdot \{1 - p_{Ex4} \operatorname{sgn}(\kappa_x)\} \cdot \lambda_{Ex} \qquad (\le 1) \tag{41}$$

$$K_x = F_z \cdot (p_{Kx1} + p_{Kx2} df_z) \cdot \exp(-p_{Kx3} df_z) \cdot \lambda_{Kx} \quad \left(= B_x C_x D_x = \frac{\partial F_{xo}}{\partial \kappa_x} \text{ at } \kappa_x = 0\right) \tag{42}$$

$$B_x = K_x / (C_x D_x) \tag{43}$$

$$S_{Hx} = (p_{Hx1} + p_{Hx2} df_z) \cdot \lambda_{Hx} \tag{44}$$

$$S_{Vx} = F_z \cdot (p_{Vx1} + p_{Vx2} df_z) \cdot \lambda_{Vx} \cdot \lambda_{\mu x} \tag{45}$$

Lateral Force (pure side slip)

$$F_{yo}^* = D_y \sin[C_y \arctan\{B_y\alpha_y - E_y(B_y\alpha_y - \arctan(B_y\alpha_y))\}] + S_{Vy} \tag{46}$$

$$\alpha_y = \alpha^* + S_{Hy} \tag{47}$$

$$\gamma_y = \gamma \cdot \lambda_{\gamma y} \tag{48}$$

$$C_y = p_{Cy1} \cdot \lambda_{Cy} \qquad (>0) \tag{49}$$

$$D_y = \mu_y \cdot F_z \tag{50}$$

$$\mu_y = (p_{Dy1} + p_{Dy2} df_z) \cdot (1 - p_{Dy3} \gamma_y^2) \cdot \lambda_{\mu y} \qquad (>0) \tag{51}$$

$$E_y = (p_{Ey1} + p_{Ey2} df_z) \cdot \{1 - (p_{Ey3} + p_{Ey4} \gamma_y) \operatorname{sgn}(\alpha_y)\} \cdot \lambda_{Ey} \qquad (\le 1) \tag{52}$$

$$K_y = p_{Ky1} F_{zo} \sin[2 \arctan\{F_z/(p_{Ky2} F_{zo} \lambda_{Fzo})\}] \cdot (1 - p_{Ky3} |\gamma_y|) \cdot \lambda_{Fzo} \cdot \lambda_{Ky}$$
$$\left(= B_y C_y D_y = \frac{\partial F_{yo}}{\partial \alpha_y} \text{ at } \alpha_y = 0\right) \tag{53}$$

$$B_y = K_y/(C_y D_y) \tag{54}$$

$$S_{Hy} = (p_{Hy1} + p_{Hy2} df_z + p_{Hy3} \gamma_y) \cdot \lambda_{Hy} \tag{55}$$

$$S_{Vy} = F_z \cdot \{p_{Vy1} + p_{Vy2} df_z + (p_{Vy3} + p_{Vy4} df_z) \gamma_y\} \cdot \lambda_{Vy} \cdot \lambda_{\mu y} \tag{56}$$

Aligning Torque (pure side slip)

$$M_{zo}^* = -t \cdot F_{yo}^* + M_{zr} \tag{57}$$

$$t(\alpha_t) = D_t \cos[C_t \arctan\{B_t \alpha_t - E_t(B_t \alpha_t - \arctan(B_t \alpha_t))\}] \cdot c_\alpha \tag{58}$$

$$\alpha_t = \alpha^* + S_{Ht} \tag{59}$$

$$M_{zr}(\alpha_r) = D_r \cos[\arctan(B_r \alpha_r)] \cdot c_\alpha \tag{60}$$

$$\alpha_r = \alpha^* + S_{Hf} \quad (= \alpha_f) \tag{61}$$

$$S_{Hf} = S_{Hy} + S_{Vy}/K_y \tag{62}$$

$$\gamma_z = \gamma \cdot \lambda_{\gamma z} \tag{63}$$

$$B_t = (q_{Bz1} + q_{Bz2} df_z + q_{Bz3} df_z^2) \cdot (1 + q_{Bz4} \gamma_z + q_{Bz5} |\gamma_z|) \cdot \lambda_{Ky}/\lambda_{\mu y} \qquad (>0) \tag{64}$$

$$C_t = q_{Cz1} \qquad (>0) \tag{65}$$

$$D_t = F_z \cdot (q_{Dz1} + q_{Dz2} df_z) \cdot (1 + q_{Dz3} \gamma_z + q_{Dz4} \gamma_z^2) \cdot (R_o/F_{zo}) \cdot \lambda_t \tag{66}$$

$$E_t = (q_{Ez1} + q_{Ez2} df_z + q_{Ez3} df_z^2) \cdot \{1 + (q_{Ez4} + q_{Ez5} \gamma_z) \arctan(B_t C_t \alpha_t)\} \qquad (\le 1) \tag{67}$$

$$S_{Ht} = q_{Hz1} + q_{Hz2} df_z + (q_{Hz3} + q_{Hz4} df_z) \gamma_z \tag{68}$$

$$B_r = q_{Bz9} \lambda_{Ky}/\lambda_{\mu y} + q_{Bz10} B_y C_y \tag{69}$$

$$D_r = F_z \cdot \{q_{Dz6} + q_{Dz7} df_z + (q_{Dz8} + q_{Dz9} df_z)\gamma_z\} \cdot R_o \cdot \lambda_{Mr} \cdot \lambda_{\mu y} \quad (70)$$

Longitudinal Force (combined) (based on [5])

$$F_x^* = D_{x\alpha} \cos[C_{x\alpha} \arctan\{B_{x\alpha}(\alpha^* + S_{Hx\alpha})\}] \quad (71)$$

$$B_{x\alpha} = r_{Bx1} \cos[\arctan(r_{Bx2}\kappa^*)] \cdot \lambda_{x\alpha} \qquad (>0) \quad (72)$$

$$C_{x\alpha} = r_{Cx1} \qquad (>0) \quad (73)$$

$$D_{x\alpha} = F_{xo} / \cos[C_{x\alpha} \arctan(B_{x\alpha} S_{Hx\alpha})] \quad (74)$$

$$S_{Hx\alpha} = r_{Hx1} \quad (75)$$

Lateral Force (combined) (based on [5])

$$F_y^* = D_{y\kappa} \cos[C_{y\kappa} \arctan\{B_{y\kappa}(\kappa^* + S_{Hy\kappa})\}] + S_{Vy\kappa} \quad (76)$$

$$B_{y\kappa} = r_{By1} \cos[\arctan\{r_{By2}(\alpha^* - r_{By3})\}] \cdot \lambda_{y\kappa} \qquad (>0) \quad (77)$$

$$C_{y\kappa} = r_{Cy1} \qquad (>0) \quad (78)$$

$$D_{y\kappa} = F_{yo} / \cos[C_{y\kappa} \arctan(B_{y\kappa} S_{Hy\kappa})] \quad (79)$$

$$S_{Hy\kappa} = r_{Hy1} \qquad (<0.1 \text{ (drive-slip)}) \quad (80)$$

$$S_{Vy\kappa} = D_{Vy\kappa} \sin[r_{Vy5} \arctan(r_{Vy6}\kappa^*)] \cdot \lambda_{Vy\kappa} \quad (81)$$

$$D_{Vy\kappa} = \mu_y F_z \cdot (r_{Vy1} + r_{Vy2} df_z + r_{Vy3}\gamma) \cdot \cos[\arctan(r_{Vy4}\alpha^*)] \quad (82)$$

Normal Load

$$F_z = \max(p_{z1} \rho \cdot \lambda_{Cz} + p_{z2} \dot{\rho} \cdot \lambda_{Kz},\ 0) \qquad (\geq 0) \quad (83)$$

Overturning Couple

$$M_x = (q_{x1} F_y + q_{x2}\gamma) \cdot F_z \cdot \lambda_{Mx} \quad (84)$$

Rolling Resistance Torque

$$M_y = \frac{2}{\pi}(q_{y1} + q_{y2}F_x)\cdot F_z \cdot \arctan V_r \cdot \lambda_{My} \tag{85}$$

Aligning Torque (combined)

$$M_z^* = -t\cdot F_y' + M_{zr} + s\cdot F_x \tag{86}$$

$$t = t(\alpha_{t,eq}) = D_t \cos[C_t \arctan\{B_t\alpha_{t,eq} - E_t(B_t\alpha_{t,eq} - \arctan(B_t\alpha_{t,eq}))\}]\cdot c_\alpha \tag{87}$$

$$F_y' = F_y^* - S_{VyK} \tag{88}$$

$$M_{zr} = M_{zr}(\alpha_{r,eq}) = D_r \cos[\arctan(B_r\alpha_{r,eq})]\cdot c_\alpha \tag{89}$$

$$s = \{s_{sz1} + s_{sz2}(F_y/F_{zo}) + (s_{sz3} + s_{sz4}df_z)\gamma\}\cdot R_o \cdot \lambda_s \tag{90}$$

$$\alpha_{t,eq} = \sqrt{\alpha_t^2 + \left(\frac{K_x}{K_y}\right)^2 \kappa^{*2}}\cdot \mathrm{sgn}(\alpha_t) \tag{91}$$

$$\alpha_{r,eq} = \sqrt{\alpha_r^2 + \left(\frac{K_x}{K_y}\right)^2 \kappa^{*2}}\cdot \mathrm{sgn}(\alpha_r) \tag{92}$$

Note that in the formulation for the pure slip aligning torque the second term of the expression (69) for B_r has been recently introduced as a replacement of the first term; the suggested value for q_{Bz10} =1.5 with q_{Bz9} =0.